RESEARCH ARTICLE

Key Points:
- An optimal estimation technique is developed for multifrequency Doppler spectra
- Dual-frequency Doppler spectra can disentangle DSD and turbulence effects
- The methodology has great potential for rain microphysics/dynamics studies

Correspondence to:
F. Tridon,
f.tridon@leicester.ac.uk

Dual-frequency radar Doppler spectral retrieval of rain drop size distributions and entangled dynamics variables

F. Tridon[1] and A. Battaglia[1,2]

[1]Earth Observation Sciences, Department of Physics and Astronomy, University of Leicester, Leicester, UK, [2]National Center Earth Observation, University of Leicester, Leicester, UK

Abstract A novel technique based on K_a-W band dual-wavelength Doppler spectra has been developed for the simultaneous retrieval of binned rain drop size distributions (DSD) and air state parameters like vertical wind and air broadening caused by turbulence and wind shear. The rationale underpinning the method consists in exploiting the peculiar features observed in Doppler spectra caused by the wavelength dependence of scattering and absorption properties. A notional study based on a large data set of DSDs measured by a two-dimensional video disdrometer demonstrates that the retrieval performs best for small/moderate air broadening spectral width and when mean volume diameters exceed at least 1 mm. The retrieval is also limited to ranges below cloud base and where the signal-to-noise ratio of both radars exceed 10 dB, which rules out regions affected by strong attenuation. Broadly speaking, it is applicable to rain rates comprised between roughly 1 and 30 mm h^{-1}. Preliminary retrieval for observations at the Atmospheric Radiation Measurement Southern Great Plains site shows very good agreement with independent reflectivity measurements from a 0.915 GHz wind profiler. The proposed methodology shows great potential in linking microphysics to dynamics in rainfall studies.

1. Introduction

Precipitation is crucially important for the availability of water for human beings, agriculture and life on Earth in general, and for its pivotal role played on the energy budget and the atmospheric circulation via the associated latent heat release. Quantitative estimations and predictions of precipitation, however, still remain one of the grand challenges in the hydrological and atmospheric sciences. Undoubtedly, an improved understanding of the temporal and spatial variability of hydrometeor size distributions and the causes for such changes represents a key step toward a physically consistent description of precipitation physics. Progress in this area calls for an orchestrated combination of models [e.g., *Seifert and Beheng*, 2001]—spectral microphysical ones in particular [e.g., *Planche et al.*, 2014]—and novel observations of the precipitating column, the topic of this research.

Since the pioneering work in the 1960s/early 1970s [*Atlas et al.*, 1973, and references therein], vertically pointing Doppler radars have been recognized as irreplaceable tools in cloud physics. Through the Fourier transform of the received signal, these radars can provide the returned radar power as function of Doppler frequency, i.e., the so-called radar Doppler spectra. Moreover, thanks to the (hydrometeor-type dependent) unambiguous relationship between particle fall speeds and sizes [*Atlas et al.*, 1973] which mirrors into an unambiguous relationship between Doppler frequency shifts and sizes, vertically pointing Doppler radars can provide range-resolved information about the size distribution of the particles contained in the radar backscattering volume. This study will specifically focus at rain and at rain drop size distribution (DSD).

Because of the dependence of raindrop fall speed on air density, the Doppler shift introduced by the vertical air velocity, and the Doppler broadening due to small-scale turbulence and cross-beam winds, it is clear that the problem of retrieving the DSD is entangled with the retrieval of air state variables like the vertical wind speed, the horizontal and vertical wind shears, the air turbulence, and the air density. *Atlas et al.* [1973] already recognized that even when updrafts are estimated to better than about ± 0.25 m s^{-1} errors in the concentration of raindrops for certain size ranges may exceed a factor of 2. The use of dual-frequency wind profiler techniques has been the classic approach to separate the air state from DSD component in radar Doppler spectra. However, the beam width of such systems is very large, and not only the nonuniform beam filling is a difficult problem to overcome but also the horizontal wind shear broadening effect can become predominant in shaping the Doppler spectra. Millimeter-wavelength radars, on the other hand, have such a narrow

beam width that broadening remains modest and is mostly due to small-scale turbulence and vertical wind shear [*Kollias et al.*, 2011]. Furthermore, at millimeter-wavelength, scattering by rain drops depends on the frequency of the transmitted wave according to the Mie theory [*Lhermitte*, 1990], and Doppler spectra from several radar frequencies can be combined to further constrain the problem.

The generalization of multifrequency Doppler radar systems, in particular at millimeter-wavelengths, e.g., in the framework of the Atmospheric Research Measurement (ARM) program [*Mather and Voyles*, 2013], offers unprecedented opportunities in rain profiling that must be fully explored. Few have attempted to exploit multifrequency millimeter-wavelength Doppler spectra observations for profiling rain microphysics so far. A technique for the separation of DSD and air state variables using the ratio of dual-wavelength Doppler spectra was proposed [*Walker and Ray*, 1974] but later abandoned facing the difficulty for obtaining good quality data [*Sangren et al.*, 1984]. The results of a recent study [*Tridon et al.*, 2013a] suggest that this technique is now applicable, thanks to the excellent quality of ARM radar Doppler spectra and the use of a more appropriate radar frequencies combination—i.e., 35–94 GHz (K_a-W bands) instead of 2.9–9.4 GHz (S-X bands). A modified version of this technique will be used as a first-order retrieval in this work. More recently, *Firda et al.* [1999] applied a spectral fitting procedure to a 33–95 GHz Doppler system spectra by using spatial and temporal continuity as a constraint. They demonstrated that such a system outperforms a single-frequency estimate and has great potential in resolving the DSDs and vertical air motion with high temporal and range resolution for stratiform and transition region rain events with rain rates between 1 and 10 mm h^{-1}.

This paper presents a novel optimal estimation framework that makes use of K_a-W band dual-frequency millimeter-wavelength radar Doppler spectra observations for retrieving rain DSD simultaneously with the vertical wind speed, the air density, and the air broadening caused by turbulence and wind shear, properly accounting for measurements and model errors and without the need of using any parameterized form for the DSD. A fundamental advantage of the retrieval is the fact that any bulk property of the DSD is retrieved via the differential attenuation technique, thus it is not affected by radar calibration or radome/antenna wetting attenuation. The optimal estimation framework is particularly suited to quantify retrieval errors and the augmented information contents when introducing observations at an additional frequency.

After a quick description of the background theory (section 2) and a review of the existing techniques and their limitations (section 3), the retrieval is presented in section 4. A notional study based on a large data set of DSD measurements describes the conditions where the retrieval shows the best performances (section 5). Finally, Rayleigh reflectivity computed from preliminary results with observations at the ARM Southern Great Plains (SGP) site shows very good agreement with independent reflectivity measurements from a 0.915 GHz wind profiler (section 6).

2. Background Theory

2.1. Radar Doppler Spectrum—Forward Model

The Doppler spectrum (e.g., see Figure 1a) observed during rain at range r by a vertically pointing radar transmitting a wave at the frequency ν can be described by (note that downward velocities are assumed positive in the following):

$$S_\nu(v, r) = A_\nu(r) \left[S_{\mathrm{rain},\nu}(v - w, r) * S_{\mathrm{air}}(v, r) \right] + S_n(r), \tag{1}$$

where $S_{\mathrm{rain},\nu}$ is the reflectivity spectrum due to scattering from rainfall, S_{air} is the air broadening kernel, w is the mean clear air vertical velocity, while $*$ represents the convolution operator. $S_n(r)$ corresponds to the noise floor and must be determined at each range gate. The factor $A_\nu = A_{\nu,\mathrm{gas}} + A_{\nu,\mathrm{rain}} + A_{\nu,\mathrm{radome}}$ is the two-way attenuation due to gases, hydrometeors, and wet radome/antenna (dB) integrated along the path from the radar to the range r.

The rainfall reflectivity spectrum $S_{\mathrm{rain},\nu}$ is proportional to the DSD $N(D, r)$ and the raindrop backscattering cross section $\sigma_{\mathrm{back},\nu}(D)$ according to

$$S_{\mathrm{rain},\nu}(v, r) = \frac{\lambda^4}{\pi^5 |\frac{\epsilon-1}{\epsilon+2}|^2} N(D, r) \sigma_{\mathrm{back},\nu}(D) \frac{\mathrm{d}D}{\mathrm{d}v}, \tag{2}$$

where ϵ is the square of the refractive index of water [*Bringi and Chandrasekar*, 2001], D is the equivolume sphere raindrop diameter and dD/dv is the derivative of drop diameter with fall speed, while the terminal fall
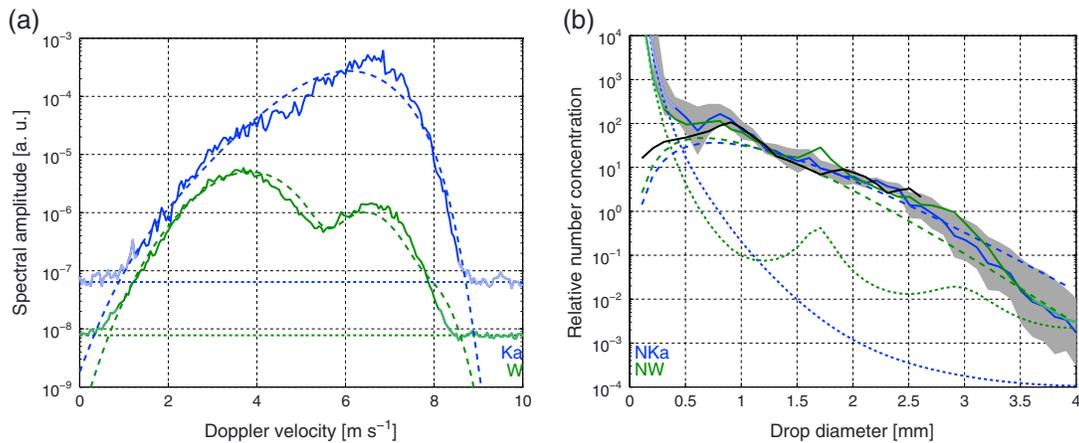
Figure 1. Example of DSD retrieval (Figure 1b, continuous and dashed blue and green lines) using K_a (Figure 1a, continuous blue line) and W band (Figure 1a, continuous green line) Doppler spectra simulated from a DSD (Figure 1b, black line) measured by the 2-D video disdrometer [*Kruger and Krajewski*, 2002] at the ARM SGP Central Facility on 24 April 2011 at 11:06 UTC. Two methods are depicted: retrieval of spectral DSDs (Figure 1b, continuous lines) from the Doppler spectra (Figure 1a, continuous lines) assuming no air broadening, retrieval of parameterized gamma DSDs (Figure 1b, dashed lines) corresponding to the best-matched forward modeled Doppler spectra (Figure 1a, dashed lines). The dotted lines represent the (a) noise floor determined by the *Hildebrand and Sekhon* [1974] technique and the corresponding (b) noise DSDs, featuring the range where the retrieved DSDs are meaningful (i.e., between 0.4 and 4.5 mm and between 0.3 and 4.0 mm for the K_a band or W band spectrum, respectively). Finally, the gray shading around the K_a band retrieved bin DSD shows the error in DSD retrieval if 0.25 m s^{-1} error is made in vertical wind estimation.

velocity of drizzle and raindrops can be uniquely parameterized following *Frisch et al.* [1995] and *Atlas et al.* [1973], respectively:

$$
v_T(D)[\text{ms}^{-1}] = \begin{cases} (41.6\,D[\text{cm}] - 0.083)\left(\dfrac{\rho_0}{\rho}\right)^{0.5} & 0.12 < D < 0.86 \text{ mm} \\ [9.65 - 10.3\exp(-6D[\text{cm}])]\left(\dfrac{\rho_0}{\rho}\right)^{0.5} & D > 0.86 \text{ mm,} \end{cases}
$$

(3)

where ρ_0 and ρ are the air densities at 1000 hPa and at the measurement altitude, respectively.

The backscattering cross sections of raindrops $\sigma_{\text{back},v}(D)$ can be computed by T-matrix method assuming an axial ratio-diameter relationship [*Beard and Chuang*, 1987]. For equivolume diameters much smaller than the wavelength λ and perfectly oriented drops, results converge to the Rayleigh theory for ellipsoids:

$$
\sigma_{\text{back}}^{\text{Ray}}(D) = \frac{\pi^5 D^6}{\lambda^4}\left|\frac{(\epsilon - 1)/3}{1 + (\epsilon - 1)L_1}\right|^2,
$$

(4)

where L_1 depends only on the axial ratio of the drops according to *Bohren and Huffman*, 1998 [1998, equation (5.34)]. Otherwise, backscattering falls into the Mie regime [*Lhermitte*, 1990] and the backscattering cross section oscillates with successive maxima and minima with increasing size and depends on the radar frequency (Figure 2). Mie effects already affect (here we consider the 20% departure from Rayleigh as a reference value) backscattering cross sections at fall velocities of 3.3 and 4.9 m s^{-1} for W and K_a band, respectively (i.e., for diameters of 0.8 and 1.3 mm).

The air broadening kernel S_{air} is typically described by a Gaussian shape [*Doviak and Zrnić*, 1993]:

$$
S_{\text{air}}(v, r) = \frac{1}{\sqrt{2\pi}\sigma_{\text{air}}(r)}\exp\left(-\frac{v^2}{2\sigma_{\text{air}}(r)^2}\right),
$$

(5)

where σ_{air} is the air broadening spectral width, which includes contributions from turbulence, crosswind, spectral window, etc. [*Doviak and Zrnić*, 1993, section 5.3].

Finally, realistic spectra are produced by adding the radar receiver white noise and by averaging M exponentially distributed realizations, where M represents the number of spectral averages, in order to produce the correct noise fluctuation [*Zrnić*, 1975; *Kollias et al.*, 2011]. This last step can be skipped if an idealized Doppler spectrum is considered.
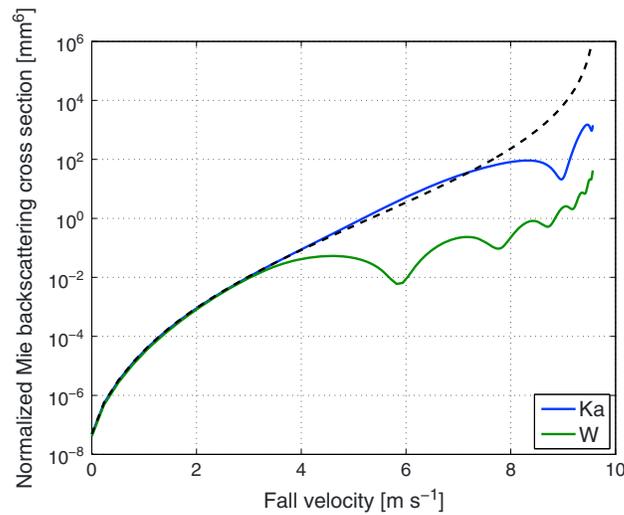
Figure 2. Raindrops backscattering cross section computed by T-matrix method for the K_a and W radar frequency bands as a function of terminal fall velocity. The values have been normalized by λ^4 in order to emphasize the Rayleigh regime (black dashed line) where K_a and W backscattering cross sections are simply scaled by the factor $\lambda_{K_a}^4 / \lambda_W^4$ (up to $v_T = 3.3$ m s^{-1}).

2.2. Rain Attenuation

The rain component of the two-way path integrated attenuation at range r $A_{v,\mathrm{rain}}(r)$ expressed in dB depends on the DSD $N(D, r)$ along the path according to

$$A_{v,\mathrm{rain}}(r) = 2 \int_0^r k_{\mathrm{ext},v}(s)\mathrm{d}s \qquad (6)$$

and

$$k_{\mathrm{ext},v}(r) = \frac{10^4}{\ln 10} \int_{D_{\min}}^{D_{\max}} N(D, r)\sigma_{\mathrm{ext},v}(D)\mathrm{d}D, \qquad (7)$$

where the factor 2 accounts for the two-way attenuation and $k_{\mathrm{ext},v}$, $\sigma_{\mathrm{ext},v}(D)$ are the attenuation coefficient (dB km^{-1}), and the individual raindrop extinction cross section (m^2), respectively.

For centimeter-wavelength radars, the rain attenuation is generally negligible at short range; and provided that the radar is well calibrated, the radar reflectivity factor measured at range r, defined as the zeroth moment of the Doppler spectrum, has a direct link with the DSD at range r.

Attenuation quickly increases with frequency, and millimeter-wavelengths are strongly affected by attenuation in heavy rain. In such cases, the reflectivity factor measured at range r depends on the DSD between the radar and range r as well, through rain attenuation. Conversely, if the DSD is approximately uniform with height, attenuation dominates the vertical gradient of reflectivities and can be used as a source of information for estimating bulk properties of precipitation. For example, climatological analyses have demonstrated that attenuation $k_{\mathrm{ext},v}$ (dB km^{-1}) is almost linearly related to rain rate R (mm h^{-1}) at K_a band ($k_{\mathrm{ext},35\mathrm{GHz}} = 0.28R$) [*Matrosov*, 2005]. At W band, the relationship is more sensitive to the DSD but can also be roughly fit by a linear relationship ($k_{\mathrm{ext},94\mathrm{GHz}} = 0.83R$, *Matrosov et al.* [2008]) with attenuation about 3 times larger than at K_a band.

3. Review of Doppler Spectra-Based DSD Retrievals

3.1. Centimeter-Wavelength Radars

The use of dual-frequency wind profiler techniques has been the classic approach to separate the air state from DSD component in radar Doppler spectra. While VHF profilers (typically operated at 50 MHz) are capable of detecting the clear air Bragg scattering, UHF profilers [*Ecklund et al.*, 1999; *Williams*, 2002] are more sensitive to hydrometeor particles (Rayleigh scattering) and are capable of resolving DSDs with mean volume diameter D_m as small as 0.5 mm [*Rajopadhyaya et al.*, 1993]. The dual-frequency profiler method [*Currier et al.*, 1992; *Schafer et al.*, 2002; *Williams*, 2012] combines the VHF profiler for measuring the clear air Doppler spectrum (hence the ambient vertical air motion and the clear air spectrum width) with the UHF profiler for measuring the spectrum of the falling precipitation. DSD are retrieved either by directly deconvolving the UHF spectra with the clear air velocity spectra or by using nonlinear least squares methods to fit an assumed function to the convolved spectra [*Schafer et al.*, 2002]. The advantage of the deconvolution over the fitting method is that it does not assume a functional form of the underlying DSD (typically a gamma distribution) and it allows a full spectral microphysics retrieval. Profiler data are now routinely used to characterize the vertical structure of precipitation systems in different regimes [e.g., *Bringi et al.*, 2009; *Williams*, 2012].

However, such retrievals are highly dependent on a good radar calibration which is a delicate task. Furthermore, the beam width of such systems is very large, and not only the nonuniform beam filling is a difficult problem to overcome but also the horizontal wind shear broadening effect can become predominant in

Table 1. Useful Specifics of the ARM SGP Radars for Doppler Spectra Simulations During the Summer 2011

Parameters	KAZR	WSACR
Frequency v (GHz)	35	94
Pulse repetition frequency (kHz)	5	9
Nyquist velocity (m s^{-1})	6	7.2
No. of point in spectra	256	256
No. of spectral average M	20	70

shaping the Doppler spectra. Finally, in order to compensate their weak sensitivity, centimeter-wavelength radars must have a coarse resolution.

3.2. Millimeter-Wavelength Radars

Millimeter-wavelength radars provide much higher spatial and temporal resolution than low-frequency systems [*Kollias et al.*, 2007]. These systems, which are primarily designed for measuring properties of nonprecipitating clouds, have also been proposed [*Lhermitte*, 1990] and exploited [*Kollias et al.*, 2002; *Matrosov et al.*, 2006] for rain profiling. The underpinning rationale is that, in presence of raindrops, millimeter-wave scattering falls into the Mie resonance region with the possibility of producing multimodal spectra (e.g., Figure 1), which can provide unique signatures of the drops sampled. For instance, the position of the first minimum in the W band backscattering cross section corresponds, at surface conditions, to a raindrop terminal velocity of 5.9 ms^{-1}. The vertical air velocity can then be deduced from the simple difference between the known terminal velocity and the position of the first resonant minimum in the spectrum with accuracies of the order of ± 0.1 m s^{-1} [*Kollias et al.*, 2002; *Giangrande et al.*, 2012].

However, the main disadvantages of millimeter-wavelength radars when observing rain is associated with the strong attenuation. Not only attenuation can reduce the radar power received from ranges beyond heavy rain layers below the noise level, but even in regions of good signal-to-noise ratio (SNR), rain retrievals require an attenuation correction, which can be very unstable in the presence of large attenuation. As a result, a DSD retrieval based on the measured (uncorrected) spectra can only produce information about the shape of the DSD $N_{\text{shape}}(D, r)$ related to the complete DSD $N(D, r)$ through an arbitrary concentration parameter $C_N(r)$ depending on attenuation and hence on range:

$$N(D, r) = C_N(r) N_{\text{shape}}(D, r). \tag{8}$$

Single wavelength techniques cannot provide bulk properties of rain like rain rate or rain water content without some limiting assumptions. On the other hand, as will be shown in section 4.2, large attenuation can be beneficial using multiwavelength radars, and several attenuation techniques have been recently proposed for the retrieval of bulk quantities [*Hogan et al.*, 2005; *Matrosov et al.*, 2006]. Being based on differential attenuation, these methodologies are not affected by the calibration of the two radars and by unknown sources of attenuation (e.g., radome wetness).

3.3. Limitations of State-of-the-Art Techniques

In order to illustrate the limitations of existing retrievals, examples of Doppler spectra under moderate broadening ($\sigma_{\text{air}} = 0.4$ m s^{-1}) and vertical wind ($w = -0.4$ m s^{-1}) conditions have been simulated at ground air density (Figure 1a) by applying the forward model described in section 2.1 with $A_{\text{Ka}} = 0$ dB and $A_W = 3$ dB and the specifics of the K$_a$ band ARM Zenith Radar (KAZR) and W-band Scanning ARM Cloud Radar (WSACR) (Table 1) to an observed DSD. From these synthetic Doppler spectra, two families of retrievals can be applied: retrieval of spectral DSDs (Figure 1b, continuous lines) from the Doppler spectra themselves or retrieval of the parameterized DSDs (Figure 1b, dashed lines) corresponding to the best-matched forward modeled Doppler spectra (Figure 1a, dashed lines). By comparison with the true DSD (Figure 1b, black line), the performances of these two traditional DSD shape retrievals can be assessed. Since these techniques are based on single millimeter-wavelength radars, they can only serve to retrieve the shape of the DSD which are then plotted in relative units.

First method. If the vertical wind is known and under the assumption of negligible spectrum broadening, the DSD shape can be simply deduced from the observed Doppler spectrum by inverting equation (2). For example, *Giangrande et al.* [2012] retrieved the DSD shape from W band radar spectra after the retrieval of vertical wind based on the position of the backscattering notches [*Kollias et al.*, 2002]. As an illustration, the first Mie notch of the W band spectrum of Figure 1a appears at a Doppler velocity of 5.5 m s^{-1}. Since the T-matrix method predicts the notch for 1.67 mm diameter drops (5.9 m s^{-1} fall velocity, Figure 2), this implies a vertical wind of -0.4 m s^{-1}. Provided that this minimum can be clearly detected—which is not always true in case

of very small D_m and/or large spectrum broadening and/or multimodal DSD—the error is of the order of the dimension of the W band Doppler velocity bins (i.e., 5.6 cm s^{-1} for the configuration of Table 1). After the vertical wind correction, the DSD shape can be retrieved from either of the spectra (Figure 1b, continuous blue and green lines). However, the retrieved DSDs may depart significantly from the observed one: for instance, as can be seen in (Figure 1b, green continuous line) and noticed by *Firda et al.* [1999], the DSD obtained from a W band spectrum corrupted by broadening can contain some anomalous humps at the diameters corresponding to the Mie notches.

Second method. In order to take into account the effect of broadening, another solution is to retrieve a parameterized DSD only: a lookup table (LUT) of Doppler spectra can be built by assuming several DSD parameters and broadening intensities, and the simulated spectrum which best matches the observations provides the DSD retrieval. In order to implement this approach, 132,000 ideal (i.e., without the noise component of the forward model) spectra were produced for each radar frequency, with three parameters (20 mean volume diameter D_m values ranging from 0.3 to 4 mm, 24 shape parameter μ values ranging from -3 to 30, and 25 maximum diameter D_{max} values ranging from 1 to 8 mm) describing the shape of a normalized gamma DSD, according to *Testud et al.* [2001] and *Williams et al.* [2014]

$$N_{shape} = \frac{6}{4^4} \frac{(4+\mu)^{\mu+4}}{\Gamma(\mu+4)} \left(\frac{D}{D_m}\right)^\mu \exp\left[-(4+\mu)\frac{D}{D_m}\right] \quad 0 < D_m < D_{max} \tag{9}$$

and 11 air broadening σ_{air} values ranging from 0.05 to 1 m s^{-1}, while w is retrieved by shifting the LUT spectra by steps of 0.1 m s^{-1}. Not only the gamma DSDs retrieved from the best matching K_a and W band spectra (Figures 1a and 1b) produce not identical results but also they are not able to fully capture the variability of this specific DSD representative of small sampling volumes.

4. DSD Two-Step Retrieval From Dual-Frequency Doppler Spectra

The examples shown in section 3.3 demonstrate that there is room for improving DSD retrievals based on multifrequency Doppler spectra. This work proposes a novel algorithm from observations of dual-frequency millimeter-wavelength radar Doppler spectra. The benefit of using such observations is twofold. First, the differences observed in the dual-frequency Doppler spectra can be used to constrain the retrieval of the DSD shape (section 4.1). Second, since the low-diameter portion of Doppler spectra corresponds to Rayleigh scattering, the K_a-W differential attenuation profile can be estimated [*Tridon et al.*, 2013b]. Hence, the full form of DSD can be retrieved (section 4.2).

4.1. Optimal Estimation Formulation for DSD Shape Retrieval

Firda et al. [1999] already noticed that multifrequency techniques have the potential of retrieving binned DSDs by properly weighting the contribution of each frequency on the diameter bins according to the SNR of each Doppler spectra bins. But ideally, a retrieval technique should also produce retrieval errors and rigorously quantify the benefit of adding a second frequency to the retrieval. Variational (also referred to as optimal estimation) methods allow one to optimize the unknowns through the matching of observations with forward model simulated spectra. They are ideal candidates for the problem under analysis since the forward modeling of the measured Doppler reflectivity spectrum corresponding to a specific rain state (DSD and dynamics) is well known and does not require any "deconvolution" step (section 2.1). Furthermore, optimal estimation allows to match both spectra while automatically accounting for the different SNR levels. The application of optimal estimation techniques has been already successfully carried out in the area of cloud/precipitation remote sensing, from nonprecipitating liquid and ice clouds profiling to rain characterization [e.g., *L'Ecuyer and Stephens*, 2002a; *Hogan*, 2007, among others]. In this work, this methodology is applied to the retrieval of a binned DSD. It is briefly summarized hereafter.

The general inverse problem consists in retrieving an unknown state vector **x** (length n) from a measurement vector **y** (length m) which is characterized by a measurement error ϵ, i.e., $\mathbf{y} = \mathbf{F}(\mathbf{x}) + \epsilon$ where **F** represents a forward operator mapping state into measured variables. It is basically achieved by minimizing the following cost function

$$CF = [\mathbf{y} - \mathbf{F}(\mathbf{x})]^T \mathbf{S}_\epsilon^{-1} [\mathbf{y} - \mathbf{F}(\mathbf{x})] + [\mathbf{x} - \mathbf{x}_a]^T \mathbf{S}_a^{-1} [\mathbf{x} - \mathbf{x}_a], \tag{10}$$

where $\mathbf{S}_\epsilon$ is the measurement error covariance matrix, $\mathbf{x}_a$ is the a priori value of $\mathbf{x}$, and $\mathbf{S}_a$ is the associated covariance matrix. The solution can be found by Newtonian iterations based on the Gauss-Newton method [*Rodgers*, 2000]:

$$\mathbf{x}_{i+1} = \mathbf{x}_i + \hat{\mathbf{S}}_i \left[\mathbf{J}_i^T \mathbf{S}_\epsilon^{-1}(\mathbf{y} - \mathbf{F}(\mathbf{x}_i)) - \mathbf{S}_a^{-1}(\mathbf{x}_i - \mathbf{x}_a) \right]. \tag{11}$$

In equation (11), $\hat{\mathbf{S}}_i = (\mathbf{S}_a^{-1} + \mathbf{J}_i^T \mathbf{S}_\epsilon^{-1} \mathbf{J}_i)^{-1}$ is the covariance matrix of the solution and $\mathbf{J}_i$ is the Jacobian of the forward operator evaluated at the i iteration of the state vector, $\mathbf{x}_i$. The problem generally converges after few iterations; a convenient convergence criterion is based on checking when the covariance-weighted square difference between successive estimates becomes much less than the number of unknowns:

$$d_i^2 = (\mathbf{x}_i - \mathbf{x}_{i+1})^T \hat{\mathbf{S}}^{-1}(\mathbf{x}_i - \mathbf{x}_{i+1}) \ll n. \tag{12}$$

The averaging kernel $\mathbf{K}_i$, defined for each iteration i as

$$\mathbf{K}_i = \hat{\mathbf{S}}_i \mathbf{J}_i^T \mathbf{S}_\epsilon^{-1} \mathbf{J}_i, \tag{13}$$

is very useful to describe an observation system. It is a linear representation of the weighting of information content of the state vector and can be used to determine the number of useful independent quantities associated to the measurements, i.e., the degree of freedom (dof), which is equal to the trace of the averaging kernel matrix $\mathbf{K}_f$ evaluated at the final iteration f [*Rodgers*, 2000].

4.1.1. State and Measurement Vectors

For the specific problem in consideration, the unknowns are the drop concentration N_j [mm^{-1} m^{-3}] for each DSD bin j and the air state variables which affect the Doppler spectra — i.e., three additional variables (namely the air broadening spectral width σ_{air} (m s^{-1}), the mean clear air vertical velocity w (m s^{-1}), and the air density ρ (kg m^{-3}) (see section 2.1) — at any desired range r (for simplicity, the dependence on the range r is implicit in the variables). Moreover, the two-way path integrated differential attenuation, ΔA (dB), due to gases, hydrometeors, and wet radome is also an unknown of the problem. This last variable also includes the relative calibration difference between the two radars which makes the technique independent of radar calibration. Accordingly, the state vector for a single range gate is

$$x = \begin{pmatrix} \log N_1 \\ \vdots \\ \log N_p \\ \log \sigma_{air} \\ w \\ \rho \\ \Delta A \end{pmatrix}. \tag{14}$$

Since N_j and σ_{air} are allowed to vary over wide intervals, the logarithm of these variables are taken in order to avoid nonphysical negative retrievals. The resolution of the DSD bins is fixed to 0.1 mm, a value close to the resolution of standard disdrometers; the number $p = n - 4$ of DSD bins, on the other hand, is not fixed and depends on the maximum diameter D_{max} selected for the retrieval (see section 4.1.4).

The measurement vector consists of each spectral reflectivity bin measured at the two frequencies at range r and interpolated on a common Doppler velocity vector of length $m/2$ with a resolution of 0.05 m s^{-1}:

$$y = \begin{pmatrix} \log S_{K_a,1} \\ \vdots \\ \log S_{K_a,m/2} \\ \log S_{W,1} \\ \vdots \\ \log S_{W,m/2} \end{pmatrix}. \tag{15}$$

4.1.2. Forward Model and Jacobian Operator

At each iteration of the Gauss-Newton method, an estimate of the observations $\mathbf{F}(\mathbf{x}_i)$ is obtained through a forward modeling operator (see equations of section 2) applied to the state vector retrieved at the previous iteration $\mathbf{x}_i$ (or from the a priori vector $\mathbf{x}_a$ at the first iteration).

The Jacobian operator $\mathbf{J}_i$ contains the partial derivative of each observation with respect to each element of the state vector, thus has a size of $m \times n$. At each iteration, $\mathbf{J}_i$ is computed numerically by the perturbation method.

4.1.3. Measurement and Model Errors

Following *Hogan et al.* [2005], the random error of measured spectral reflectivity can be expressed as

$$\Delta S(v) = S(v) \left[\frac{1}{M_i} + \frac{1}{M} \left(\frac{1}{\mathrm{SNR}(v)^2} + \frac{2}{\mathrm{SNR}(v)} \right) \right], \tag{16}$$

where $\mathrm{SNR}(v)$ is the SNR of the spectral reflectivity in the velocity bin centered on v, M is the number of spectral averages, and M_i is the number of independent samples ($M_i < M$) and depends on radar frequency and spectrum width.

The forward model (section 2.1) is a simplified mathematical description of the measurement. The most important error source in the spectra modeling is believed to consist in the use of a fixed diameter-fall velocity relationship. Indeed, after interactions with other drops (collision, coalescence, and breakup), individual drops require some time to reach their terminal velocity. Furthermore, the drop shapes oscillate and can lead to a slight dispersion in drop terminal velocity for a given size. These errors are estimated from the difference between two spectra simulated using modified $D\text{-}v_{\mathrm{fall}}$ relations where the velocities are perturbed by ± 0.1 m s^{-1}. This results in increased errors on the flanks of the spectra and at largest fall velocities where the $D\text{-}v_{\mathrm{fall}}$ relation starts to saturate (i.e., the parameterization of equation (3) reaches an asymptote for fall velocities of 9.65 m s^{-1}).

4.1.4. A Priori and Its Covariance

Like for any underconstrained retrieval, multiple solutions for the unknowns vectors are possible. Therefore, a good a priori vector (which in the present case coincides with the starting point of the iteration process) is extremely important so that the retrieval converges to the right solution. Generally, the a priori vector is a climatological "average" of the unknowns, while the associated covariance matrix represents the climatological variability around this average. However, it is well documented that the DSDs exhibit strong spatial and temporal variability and an a priori encompassing all the possible DSDs would be a very poor constraint on the retrieval. The alternative, as proposed by *L'Ecuyer and Stephens* [2002b], is to use a two-step retrieval where a traditional DSD inversion technique provides a first guess which can then be used both as an a priori and an initial condition for the iterative scheme.

It is proposed here to derive an a priori by the extension of the Doppler spectral ratio (DSR) technique [*Tridon et al.*, 2013a]. Under no turbulence and no wind shear conditions, the DSR reduces to a universal shape (black dashed line in Figure 3) proportional the ratio of the backscattering cross sections

$$\mathrm{DSR}(v,r) = \frac{S_{K_a}(v,r)}{S_W(v,r)} = \frac{\lambda_{K_a}^4}{\lambda_W^4} \frac{\sigma_{\mathrm{back},K_a}(D,r)}{\sigma_{\mathrm{back},W}(D,r)}; \tag{17}$$

changes in the vertical wind w and differential attenuation ΔA simply shift the full curve along the Doppler velocity and the DSR axis, respectively. On the other hand, air broadening affects the rainfall power spectra according to their initial shape; and as a result, the DSR in presence of turbulence or wind shear depends on the broadening intensity and on the DSD (continuous lines in Figure 3). Then, in the same way as *Moisseev and Chandrasekar* [2007], the measured spectra can be individually deconvolved with various turbulence intensities [*Lucy*, 1974], and their

Figure 3. Schematic of the effect of vertical wind, differential attenuation, and broadening on the DSR.

Figure 4. (a–c) Illustration of optimal estimation of the DSD shape from the Doppler spectra of Figure 1.

ratios can be matched to the universal DSR shape in order to retrieve simultaneously σ_{air}, w, and ΔA.

The deconvolved spectra corresponding to the retrieved σ_{air} provide estimates of the DSD (the gamma fit of the K_a band retrieved DSD is actually used as DSD a priori for all diameter bins), while its deviation from a DSD deduced directly from the spectra under the no turbulence assumption (like in Figure 1) provides estimate of the standard deviation of the a priori DSD, i.e., the diagonal terms of the covariance matrix. Nondiagonal terms are set assuming a 1 mm correlation length between the drop number concentration. The standard deviations of $\log(\sigma_{air})$, w, and ΔA are set to intentionally large values of 0.5 m s^{-1}, 0.2 m s^{-1}, and 10 dB, respectively, while the corresponding off diagonal terms are all zero since these parameters are all independent. A priori for ρ is derived from surface measurements corrected for the measurement altitude. It is well defined and has only been added to the unknowns in order to give some flexibility to the retrieval but with a very low standard deviation of 0.01 kg m^{-3}.

Finally, D_{max} is taken as 2.5 times D_m of this a priori DSD. If larger drops are contributing to the measured spectra, the retrieval does not converge or converge to a wrong solution with very large σ_{air} and poor CF. In such cases, D_{max} is increased by steps of 1 mm until convergence is obtained with $\sqrt{CF/(n+m)}$ lower than 0.25 [−] (i.e., until the retrieved parameters are within a quarter of their allowed standard deviation in average) in order to ensure that convergence is meaningful when it is found.

4.1.5. Example of Retrieval

Figure 4 illustrates the DSD shape retrieval when adopting the variational algorithm from the spectra depicted in Figure 1. For completeness, the spectra are replotted with the corresponding combined measurement and model errors (Figures 4a and 4b, black lines and gray shadings) as well as the "true" DSD which was used to produce these spectra (Figure 4c, black line). The blue line and the blue shading in Figure 4c represent the a priori first guess and standard deviation, respectively. The K_a and W band Doppler spectra corresponding to this first guess (blue lines in Figures 4a and 4b) illustrate the limited accuracy of the technique used to derive the a priori with only reasonable agreement with the true

spectra. This is expected primarily because of the inaccuracy of a deconvolution applied to noisy spectra and highlights the necessity of the variational algorithm. The other colored lines represent the Doppler spectra and DSD shape at each iteration. Convergence is quickly found after the sixth iteration. The variance of the retrieved DSD (cyan shading in Figure 4c) shows a clear improvement compared to the variance of the a priori, while the retrieved DSD shape (cyan line) is almost spot-on with the true DSD (continuous black line). Note that absolute concentration is retrieved only because A_{Ka} was assumed to be null in the Doppler spectra simulations. Finally, the other retrieved parameters are in good agreement with the values used for the simulation (legend of Figure 4c).

4.2. Bulk Properties of the DSD

The first step of the retrieval provides profiles of DSD shape, $N_{shape}(D, r)$, and two-way differential attenuation $\Delta A(r)$. These two quantities are complementary for a complete DSD description. Since any calibration or radome attenuation factor cancels out, the differential attenuation change within a layer is only related to the gas and hydrometeors present in that layer. The range derivative of $\Delta A_{rain}(r)$ is related to the DSD shape through the arbitrary concentration parameter $C_N(r)$ (equation (8)):

$$\frac{d\left(\Delta A_{rain}(r)\right)}{dr} = 2\frac{10^4}{\ln 10}C_N(r)\int_0^{D_{max}} N_{shape}(D, r)\left(\sigma_{ext,v2}(D) - \sigma_{ext,v1}(D)\right)dD \tag{18}$$

where $v_1 < v_2$ are the frequencies of the radars. Then equation (18) gives the unknown coefficient $C_N(r)$ and equation (8) gives the complete DSD and from the latter, any DSD moment can be derived (e.g., rain water content, RWC, rain rate, R, or reflectivity factor, Z).

In the retrieval, first the differential attenuation is fitted with a monotonically increasing function, then the range derivative of the two-way rain differential attenuation component $\Delta A_{rain}(r)$ is computed for each layer by subtracting the gas contribution, estimated from the closest sounding measurement. Note that here the cloud contribution is neglected, which may contribute to a significant underestimation of the rain rates. Ancillary measurements with collocated lidar can actually be used to identify the presence of such layer and screen out data above cloud base.

5. Performance of DSD Shape Retrieval on Synthetic Data

In order to assess the retrieval uncertainty, 2230 one minute DSD measured by the ARM SGP two-dimensional video disdrometer corresponding to 18 different rain events between April and October 2011 were used to simulate an ensemble of realistic radar Doppler spectra. These simulations allow to compute statistics (e.g., biases and standard deviations) of the retrieved parameters σ_{air}, w, and ΔA. Furthermore, the mass spectrum mean diameter, D_m, and the mass spectrum standard deviation, σ_m, are used to describe the mean value and width of any distribution without the need of any assumption of a parametric shape [*Williams et al.*, 2014].

In addition to the DSD, the air spectral broadening σ_{air} and the signal-to-noise ratio (SNR) are the essential parameters affecting the shape of the Doppler spectra; these parameters have been changed in order to assess the quality of the retrieval in different regions of the state vector space.

5.1. Range of D_m and σ_{air} for Optimal Performances

The mean bias of the retrieved parameters as function of D_m (black lines in Figure 5) indicates the quality of the retrieval according to the general shape of the DSD, while the standard deviation (shaded area or error bars) gives an insight on the uncertainty provided by specific details of individual DSD shape. It is assumed that the general shape of the DSD is well represented by D_m since σ_m is statistically very well correlated with D_m [*Williams et al.*, 2014]. Furthermore, for each DSD, several spectra were simulated using various σ_{air} in order to assess the influence of the air broadening. For low σ_{air}, the quality of all the retrieved parameters is very good with very low bias and standard deviation (continuous black line and error bars in Figure 5) down to D_m=1 mm. Below that threshold, the Mie effects are too weak to produce significantly different Doppler spectra between the two radar frequencies, an essential requirement without which the vertical wind cannot be properly corrected. For larger σ_{air} (dashed black line and shaded area in Figure 5), the quality of the retrieval slowly degrades with increasing biases and standard deviations and a reduced domain of validity retrievals becoming accurate only at mean volume diameter larger than 1.25 mm. This is attributed to the smoothing effect of the Mie features associated to increased values of σ_{air}. Overall, for $D_m > 1$ mm and $\sigma_{air} < 0.75$ m s^{-1}, both standard deviations and absolute biases are expected to be lower than 0.07 mm for D_m, 0.1 mm for σ_m, 0.1 m s^{-1} for w, 0.1 m s^{-1} for σ_{air}, and 1 dB for ΔA.
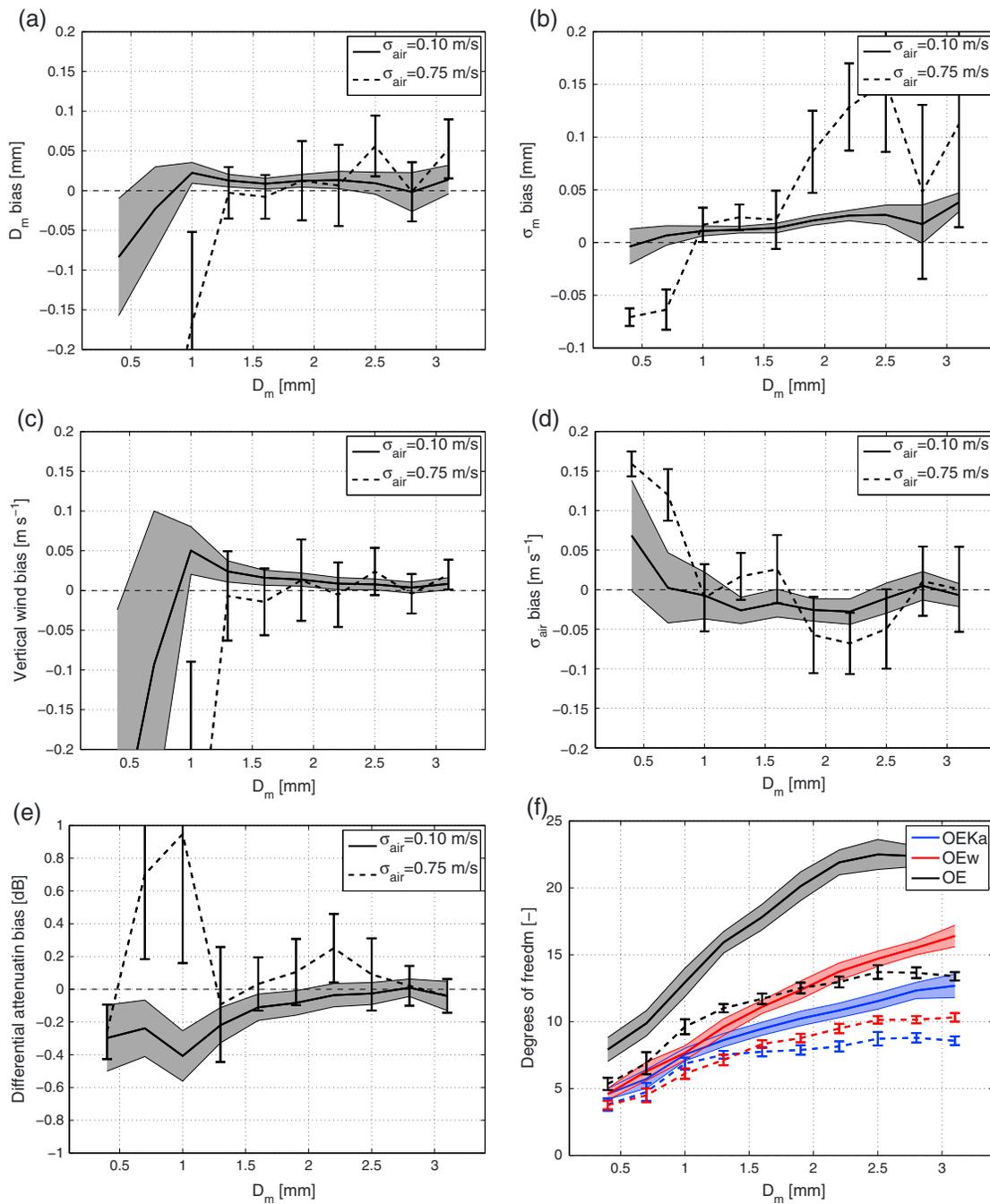
Figure 5. Precision and accuracy (biases and standard deviations) of the retrieved (a) D_m, (b) σ_m, (c) w, (d) σ_{air}, and (e) ΔA as function of D_m and σ_{air}. (f) Degrees of freedom of the retrieval using one or two frequencies.

5.2. Performance as Function of SNR

The sensitivity study of section 5.1 was made in an ideal case of very good SNR (30 and 20 dB for the K_a and W band spectrum, respectively), where the noise is defined as mean reflectivity across spectral bins free of echo and the signal is the sum of all remaining bins. However, the SNR can be much lower in case of very low signal due to light rain or drizzle or due to attenuation of the signal caused by heavy rain. Within the domain of best performances determined previously ($D_m > 1$ mm and low σ_{air}), the sensitivity to SNR was assessed by simulating various SNR ranging from 0 to 30 dB for both spectra (Figure 6). The attenuation at W band is generally much higher than at K_a band, so only two extreme cases were considered for simplification: a situation with similar attenuations at both frequencies (same SNR for both radars, continuous black line and
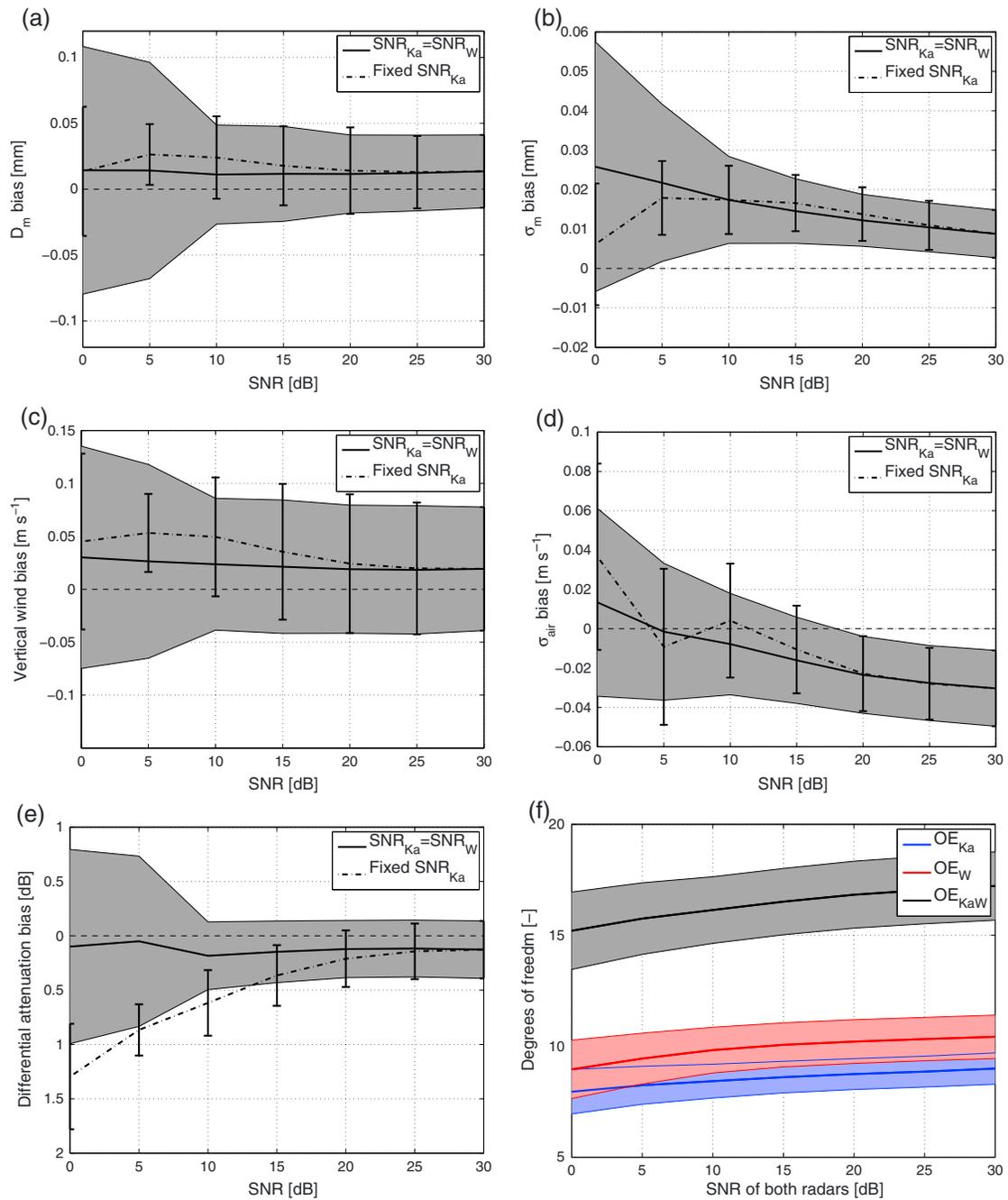
Figure 6. Precision and accuracy (biases and standard deviations) of the retrieved (a) D_m, (b) σ_m, (c) w, (d) σ_{air}, and (e) ΔA as function of SNR. (f) Degrees of freedom of the retrieval using one or two frequencies.

shaded area) and a situation with heavy attenuation at W band only while the K_a band SNR is fixed at 30 dB (dash dotted line and error bars). At 30 dB, the two cases are equivalent and the curves merge. When the SNR tends toward low values, the accuracy of the retrieval decreases substantially, in particular when the SNR of both radars is low. As a rule of thumb, we can conclude that, when selecting the optimal range for D_m and σ_m, the retrieval provides good performances when the SNRs of both radars exceed 10 dB.

5.3. Benefit Brought by an Additional Frequency

Optimal estimation allows assessing the added information content brought by a second frequency. The degrees of freedom (dof, section 4.1) describes the number of useful independent quantities associated to

Figure 7. Profile of (a) K_a and (b) W band spectra and (c) corresponding retrieved binned DSD.

the measurements. For instance, the different bins of a Doppler spectrum are correlated so that the dof can be significantly lower than the number of measurements. A single-frequency version of the optimal estimation has been implemented and the dof associated with the single- and dual-frequency retrievals have been compared.

The benefit of the dual-frequency approach is demonstrated with a dof which is significantly higher than for the single-frequency ones (Figures 6f and 5f). It is sensible that the W band single-frequency version has always a larger dof than its K_a band counterpart because of the more pronounced Mie features in W band spectra. Furthermore, the dof tends to increase with SNR and D_m since the corresponding spectra becomes wider. Finally, when σ_{air} increases, the dof decreases since the Doppler spectra bins become more correlated.

6. Example on a Case Study

The retrieval has been applied to a rain profile measured at the ARM SGP site by the K_a band (KAZR) and W band (WSACR) radars on the 12 June 2011 at 06:06:15 UTC. Collocated lidar measurements confirm that the retrieval can be performed since this profile was free of any cloud layer up to 2.5 km (not shown). First of all, a common height vector has been created using the radar with the lowest height resolution and selecting the spectra closest to each gate. A profile of a selection of these gates (Figures 7a and 7b) shows an interesting variability and demonstrates the richness of information provided by radar Doppler spectra. Several features can be noticed: (1) the spectra are widening with height probably because of the reduced air density and the corresponding increase in raindrop fall speed but possibly because of evaporation as well; (2) some spectra are shifted on the Doppler velocity axis presumably because of vertical wind variability; (3) contrary to the K_a band, the magnitude of the W band spectra is decreasing with height as expected with rain producing heavy attenuation at W band; (4) a layer of wide spectra (around 1300 m) is produced by wider DSDs as opposed to a layer of very wide spectra (around 1500 m) caused by heavy air broadening as inferable from the presence or disappearance of the W band Mie notch.

Figure 8. A priori mean (blue continuous line) and standard deviation (horizontal blue bars) and retrieved mean (red dash line) and standard deviation (red shading) profiles of (a) w, (b) σ_{air}, (c) ΔA, and (d) D_m and σ_m.

The first step of the retrieval described in section 4.1 has been applied to each range gate independently. The retrieved profiles are compared to their a priori in Figures 8a–8d. The overall good vertical continuity of the retrieved parameters (in particular a quasi-monotonically increasing differential attenuation) is a first indication of the consistency of the retrieval. The retrieved DSD shape (Figure 7c) confirms a wider DSD around 1300 m, while the retrieved parameters (Figures 8a–8c) showcase a highly dynamic layer with large σ_{air} and vigorously varying w between 1500 and 2000 m (note that an updraft is defined with positive velocities and that this precipitation profile was associated with downward wind velocities). Furthermore, Figures 8a–8d highlight the improvement brought by the variational method compared to the a priori (D_m and σ_m errors are omitted since they almost span the whole axis of Figure 8d). From the large error of the a priori (see section 4.1.4), the measurements constrain the retrieval to very low errors. On the other hand, given its low a priori standard deviation, the air density retrieval is very close to its a priori (not shown).

After monotonically fitting the total differential attenuation ΔA (dashed black line of Figure 8c) and calculating the two-way gas attenuation (which does not exceed 2 dB through the whole layer), the differential attenuation due to rain ΔA_{rain} can be deduced (dashed green line) and the bulk rain properties can be derived by applying equation (18). The computed DSD moments (Figures 9a and 9b) have a reasonable error mostly associated to the DSD shape error. This example clearly demonstrates the potential of K_a-W Doppler radar observations for characterizing rain dynamics and microphysics for a profile including rain rates up to 10 mm/h. The W band SNR at the top of this 3.5 km thick rain layer is 0 dB; the same level of signal can be achieved in presence of even higher rain rates but for thinner rain layers.

A number of technical issues could deteriorate the quality of the retrieval. In particular, techniques combining the Doppler spectra from different radars like these ones rely on a very good matching of the sampling
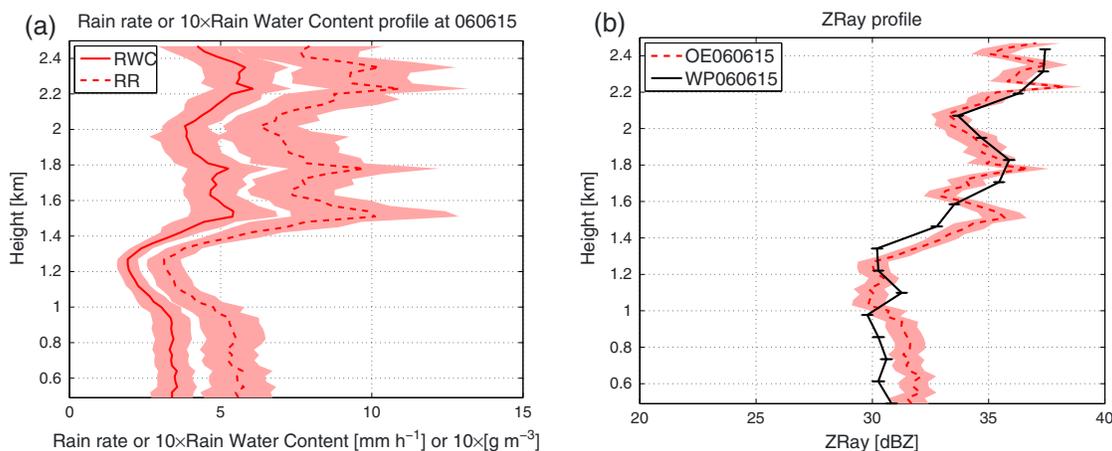
Figure 9. Retrieved profiles of (a) R and RWC, and (b) Rayleigh reflectivity compared with measured wind profiler reflectivity.

volumes. The fact that convergence is easily found for the whole profile with realistic DSD shapes is a proof that the beam matching of the radars was fairly good for this profile. However, these issues must be checked from case to case because the configuration can slightly change over time. In the future, the use of the last generation of dual-wavelength scanning ARM cloud radars will guarantee good matching of the sampling volume in range, time, and pointing.

A comprehensive intercomparison study with other independent retrievals and in situ measurements is scope of future research. However, the independent measurements of the collocated ARM 0.915 GHz wind profiler (WP) [*Tridon et al.*, 2013a] can be used to assess the consistency of the retrievals. From WP reflectivity measured for this profile ($Z_{WP} = 30 - 37$ dBZ), the widely used $Z_{Ray} = 200R^{1.6}$ relation predicts a range of rain rates $R = 3 - 9$ mm h^{-1} in good agreement with the retrievals (Figure 9a). Conversely, the Rayleigh radar reflectivity (i.e., the sixth moment of the DSD) associated with the retrieved profile can be computed and compared with WP measurements. Despite the mismatch between the sampling volume of the radars (9° for the WP versus 0.3° 3 dB beam-width antenna for the K$_a$ and W band radars), the profile of the forward modeled Rayleigh reflectivity factor shows a very good agreement with the WP reflectivity with less than 2 dB difference (Figure 9b). The error bars represent the random error of the reflectivity measured by the wind profiler following the uncertainties provided by equation (16).

7. Conclusions

A new technique has been developed for the retrieval of binned rain drop size distributions from K_a and W band dual-wavelength Doppler spectra. Its novelty resides in the explicit retrieval of the air broadening due to turbulence and wind shear. The benefit of using two radar frequencies is twofold: first, the Mie peculiar features observed in Doppler spectra at the two frequencies are optimally matched by a variational method and allow to retrieve the drop size distribution shape and disentangle air state parameters like vertical wind and air broadening; second, the differential attenuation along the path can be exploited to retrieve bulk rain quantities independently from the absolute calibration of the two radars. The latter stage requires a collocated lidar in order to screen out data above cloud base.

It has been demonstrated from a synthetic study that the retrievals should optimally perform for air broadening spectrum widths smaller than 0.75 m s^{-1}, drop size distributions with a mean volume diameter larger than 1 mm and where the W band signal is characterized by signal-to-noise ratios (SNR) higher than 10 dB which excludes the possibility of applying the retrieval at high rain rates. For instance, a 3 (1) km thick rainfall layer with $R = 10$ (30) mm/h produces roughly a two-way attenuation of 50 dB, which when coupled with W band reflectivities at high rain rates (25/30 dBZ) and with typical radar sensitivity of W band ground-based systems ($-30/-35$ dBZ in the first kilometers) keeps the SNR at acceptable levels for the retrieval to be effective. In first approximation, the two-way differential attenuation is related to rain rate through ΔA (dB km^{-1}) $= 1.1R$ (mm h^{-1}) (see aforementioned values of attenuation at the end of section 2). Assuming that the minimum detectable ΔA is 1 dB km^{-1}, this retrieval is applicable to rain rates comprised between roughly 1 and 30 mm h^{-1}.

While a thorough validation will be the object of future studies, the retrieval has been applied to a profile of stratiform rain with embedded convection: results show very good agreement with the independent reflectivity measured by a collocated wind profiler. The retrieved values of air broadening are not negligible and highlight the potential of the proposed retrieval in identifying interesting structures even in moderate rain cases, when the variability of the dynamic conditions may contrast with the smoothness of the rain microphysics.

The methodology can be extended to other frequency combinations, e.g., by including additional systems in the X band and/or in the G band [*Battaglia et al.*, 2014], which could lead to a seamless retrieval of the precipitating column from light drizzle to heavy rainfall. This approach opens the door to a variety of applications ranging from the characterization of the spatio-temporal variability of rain in the vertical column—useful for testing the assumptions underpinning rain retrieval algorithms for spaceborne radars—to identifying fingerprints of rain microphysical processes like coalescence and breakup—and thus ultimately to improving rain parametrizations in cloud models.

References

Atlas, D., R. C. Srivastava, and R. S. Sekhon (1973), Doppler radar characteristics of precipitation at vertical incidence, *Rev. Geophys.*, *11*, 1–35.

Battaglia, A., C. D. Westbrook, S. Kneifel, P. Kollias, N. Humpage, U. Löhnert, J. Tyynelä, and G. W. Petty (2014), G-band (140–220 GHz) atmospheric radars: New frontiers in cloud physics, *Atmos. Meas. Tech.*, *7*, 1527–1546.

Beard, K. V., and C. Chuang (1987), A new model for the equilibrium shape of raindrops, *J. Atmos. Sci.*, *44*, 1509–1524.

Bohren, C. F., and D. R. Huffman (1998), *Absorption and Scattering of Light by Small Particles*, 544 pp., Wiley, New York.

Bringi, V. N., and V. Chandrasekar (2001), *Polarimetric Doppler Weather Radar, Principles and Applications*, 636 pp., Cambridge Univ. Press, Cambridge.

Bringi, V. N., C. R. Williams, M. Thurai, and P. T. May (2009), Using dual-polarized radar and dual-frequency profiler for DSD characterization: A case study from Darwin, Australia, *J. Atmos. Oceanic Technol.*, *26*, 2107–2122.

Currier, P. E., S. K. Avery, B. B. Balsley, K. S. Gage, and W. L. Ecklund (1992), Combined use of 50 MHz and 915 MHz wind profilers in the estimation of raindrop size distributions, *Geophys. Res. Lett.*, *19*, 1017–1020.

Doviak, R. J., and D. S. Zrnić (1993), *Doppler Radar and Weather Observations*, 562 pp., 2nd ed., Academic Press, San Diego, Calif.

Ecklund, W. L., C. R. Williams, P. E. Johnston, and K. S. Gage (1999), A 3-GHz profiler for precipitating cloud studies, *J. Atmos. Oceanic Technol.*, *16*, 309–322.

Firda, J. M., S. M. Sekelsky, and R. E. McIntosh (1999), Application of dual-frequency millimeter-wave doppler spectra for the retrieval of drop size distributions and vertical air motion in rain, *J. Atmos. Oceanic Technol.*, *16*, 216–236.

Frisch, A. S., C. W. Fairall, and J. B. Snider (1995), Measurement of stratus cloud and drizzle parameters in ASTEX with a K_α-band Doppler radar and a microwave radiometer, *J. Atmos. Sci.*, *52*, 2788–2799.

Giangrande, S. E., E. P. Luke, and P. Kollias (2012), Characterization of vertical velocity and drop size distribution parameters in widespread precipitation at ARM facilities, *J. Appl. Meteorol. Climatol.*, *51*, 380–391.

Hildebrand, P. H., and R. S. Sekhon (1974), Objective determination of the noise level in Doppler spectra, *J. Appl. Meteorol.*, *13*, 808–811.

Hogan, R. J. (2007), A variational scheme for retrieving rainfall rate and hail reflectivity fraction from polarization radar, *J. Appl. Meteorol. Climatol.*, *46*, 1544–1564.

Hogan, R. J., N. Gaussiat, and A. J. Illingworth (2005), Stratocumulus liquid water content from dual-wavelength radar, *J. Atmos. Oceanic Technol.*, *22*, 1207–1218.

Kollias, P., B. Albrecht, and F. Marks (2002), Why Mie? Accurate observations of vertical air velocities and raindrops using a cloud radar, *Bull. Am. Meteorol. Soc.*, *83*, 1471–1483.

Kollias, P., E. E. Clothiaux, M. A. Miller, B. A. Albrecht, G. L. Stephens, and T. P. Ackerman (2007), Millimeter-wavelength radars: New frontier in atmospheric cloud and precipitation research, *Bull. Am. Meteorol. Soc.*, *88*, 1608–1624.

Kollias, P., J. Rémillard, E. Luke, and W. Szyrmer (2011), Cloud radar Doppler spectra in drizzling stratiform clouds: 1. Forward modeling and remote sensing applications, *J. Geophys. Res.*, *116*, D13201, doi:10.1029/2010JD015237.

Kruger, A., and W. F. Krajewski (2002), Two-dimensional video disdrometer: A description, *J. Atmos. Oceanic Technol.*, *19*, 602–617.

L'Ecuyer, T. S., and G. L. Stephens (2002a), An estimation-based precipitation retrieval algorithm for attenuating radars, *J. Appl. Meteorol.*, *41*, 272–285.

L'Ecuyer, T. S., and G. L. Stephens (2002b), An estimation-based precipitation retrieval algorithm for attenuating radars, *J. Appl. Meteorol. Climatol.*, *41*, 272–285.

Lhermitte, R. (1990), Attenuation and scattering of millimeter wavelength radiation by clouds and precipitation, *J. Atmos. Oceanic Technol.*, *7*, 464–479.

Lucy, L. B. (1974), An iterative technique for the rectification of observed distributions, *Astron. J.*, *79*, 745–754.

Mather, J. H., and J. W. Voyles (2013), The ARM climate research facility: A review of structure and capabilities, *Bull. Am. Meteorol. Soc.*, *94*, 377–392.

Matrosov, S. Y. (2005), Attenuation-based estimates of rainfall rates aloft with vertically pointing Ka-Band radars, *J. Atmos. Oceanic Technol.*, *22*, 43–54.

Matrosov, S. Y., P. T. May, and M. D. Shupe (2006), Rainfall profiling using atmospheric radiation measurement program vertically pointing 8-mm wavelength radars, *J. Atmos. Oceanic Technol.*, *23*, 1478–1491.

Matrosov, S. Y., A. Battaglia, and P. Rodriguez (2008), Effects of multiple scattering on attenuation-based retrievals of stratiform rainfall from cloudSat, *J. Atmos. Oceanic Technol.*, *25*, 2199–2208.

Moisseev, D. N., and V. Chandrasekar (2007), Nonparametric estimation of raindrop size distributions from dual-polarization radar spectral observations, *J. Atmos. Oceanic Technol.*, *24*, 1008–1018.

Planche, C., W. Wobrock, and A. I. Flossmann (2014), The continuous melting process in a cloud-scale model using a bin microphysics scheme, *Q. J. R. Meteorol. Soc.*, *140*, 1986–1996.

Rajopadhyaya, D. K., P. T. May, and R. A. Vincent (1993), A general approach to the retrieval of raindrop size distributions from wind profiler Doppler spectra: Modeling results, *J. Atmos. Oceanic Technol.*, *10*, 710–717.

Rodgers, C. D. (2000), *Inverse Methods for Atmospheric Sounding: Theory and Practice*, 238 pp., World Sci., London.

Sangren, K. L., P. S. Ray, and G. B. Walker (1984), A comparison of techniques to estimate vertical air motions and raindrop size distributions, *J. Atmos. Oceanic Technol.*, *1*, 152–165.

Schafer, R., S. Avery, P. May, D. Rajopadhyaya, and C. Williams (2002), Estimation of rainfall drop size distributions from dual-frequency wind profiler spectra using deconvolution and a nonlinear least squares fitting technique, *J. Atmos. Oceanic Technol.*, *19*, 864–874.

Seifert, A., and K. D. Beheng (2001), A double-moment parameterization for simulating autoconversion, accretion and self-collection, *Atmos. Res.*, *59*, 265–281.

Testud, J., S. Oury, R. A. Black, P. Amayenc, and X. Dou (2001), The concept of 'normalized' distribution to describe raindrop spectra: A tool for cloud physics and cloud remote sensing, *J. Appl. Meteorol. Climatol.*, *40*, 1118–1140.

Tridon, F., A. Battaglia, P. Kollias, E. Luke, and C. R. Williams (2013a), Signal postprocessing and reflectivity calibration of the atmospheric radiation measurement program 915-MHz wind profilers, *J. Atmos. Oceanic Technol.*, *26*, 1120–1134.

Tridon, F., A. Battaglia, and P. Kollias (2013b), Disentangling Mie and attenuation effects in rain using a K_a-W dual-wavelength Doppler spectral ratio technique, *Geophys. Res. Lett.*, *40*, 5548–5552, doi:10.1002/2013GL057454.

Walker, G. B., and P. S. Ray (1974), Precipitation characteristics at vertical incidence from multiple wavelength Doppler radars, *J. Atmos. Sci.*, *31*, 1948–1948.

Williams, C. R. (2002), Simultaneous ambient air motion and raindrop size distributions retrieved from UHF vertical incident profiler observations, *Radio Sci.*, *37*, 1024–1039.

Williams, C. R. (2012), Vertical air motion retrieved from dual-frequency profiler observations, *J. Atmos. Oceanic Technol.*, *29*, 1471–1480.

Williams, C. R., et al. (2014), Describing the shape of raindrop size distributions using uncorrelated raindrop mass spectrum parameters, *J. Appl. Meteorol. Climatol.*, *53*, 1282–1296.

Zrnić, D. S. (1975), Simulation of weatherlike doppler spectra and signals, *J. Appl. Meteorol.*, *14*, 619–620.